Journal of ELECTRONIC MATERIALS, Vol. 37, No. 1, 2008 *Special Issue Paper*
DOI: 10.1007/s11664-007-0281-7
© 2007 TMS

The Influence of 0–0.1 wt.% Ni on the Microstructure and Fluidity Length of Sn-0.7Cu-*x*Ni

TINA VENTURA,[1,4] CHRISTOPHER M. GOURLAY,[1] KAZUHIRO NOGITA,[1] TETSURO NISHIMURA,[2] MICHEL RAPPAZ,[3] and ARNE K. DAHLE[1]

1.—Materials Engineering, The University of Queensland, Brisbane, QLD 4072, Australia. 2.—Nihon Superior Company Ltd., 1-16-15 Esaka-Cho, Suita, Osaka 564-0063, Japan. 3.—Computational Materials Laboratory, Institute of Materials, School of Engineering, Ecole Polytechnique Federale de Lausanne, Station 12, 1015 Lausanne, Switzerland. 4.—e-mail: t.ventura@uq.edu.au

Alloys based on the Sn-0.7Cu-*x*Ni system are potential Pb-free solders. In this paper we report on the solidification characteristics and microstructures of Sn-0.7Cu alloys containing 0–1,000 ppm nickel. The microstructural observations show that increasing the nickel content reduces the volume fraction of primary Sn, thus generating a more-eutectic microstructure. In an attempt to better understand the changes in solderability with Ni additions, fluidity tests were carried out using the Ragone method for small incremental increases in nickel content. The maximum fluidity length was found to vary strongly with nickel content. Additionally, the distribution of nickel within samples was investigated using synchrotron micro X-ray fluorescence.

Key words: Eutectic, solidification, lead-free soldering, Sn-Cu alloys, nickel, fluidity

INTRODUCTION

For the last 50 years, electronic circuit boards have been effectively soldered with the Sn-37Pb eutectic alloy. In recent years, environmental legislation has targeted the widespread use of lead in the electronics industry because of its toxicity, thus forcing the industry to develop competitive replacement solder alloys.[1] Although there has been a concerted effort to develop lead-free solders, the search for an optimum replacement is ongoing.[1–7]

One potential lead-free solder is the near-eutectic Sn-0.7Cu alloy (all compositions are in wt.%), which has found applications in wave, dip, and iron soldering processes and presents cost advantages compared to Ag-containing alternatives.[8,9] It has been discovered that the addition of 20–1,000 ppm Ni improves the soldering properties of the Sn-0.7Cu alloy,[10–12] including a reduced tendency for bridging, a better solder-substrate interface, and an improved surface finish. For example, Fig. 1 shows that the Sn-0.7Cu alloy containing 600 ppm Ni can successfully solder a 0.5 mm pitch without bridging. Based on this improved soldering performance, the Sn-0.7Cu-*x*Ni system has become one of the most promising lead-free solders, although detailed studies of the solidification and phase equilibria are only just beginning.

In developing a Pb-free replacement alloy for wave soldering, it is important to find an alloy that is able to flow easily on the circuit board and for the excess material to drain away leaving only tidy fillets. Partial solidification is expected to occur during wave soldering because the solder is at low superheat at the start of the process and the circuit board is cool relative to the liquidus temperature of the solder. The draining of excess material is therefore the flow of partially solidified solder. The extent to which an alloy can flow as it solidifies can be studied using a maximum fluidity length test[13,14] in which a liquid alloy is forced to flow through a relatively cold tube so that the alloy solidifies as it flows.

The present study further investigates the effect of nickel content on the solidification behavior and

(Received March 15, 2007; accepted August 13, 2007; published online September 19, 2007)

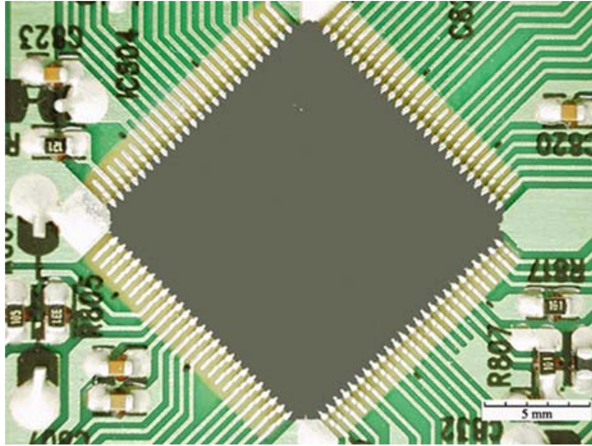

Fig. 1. Photo of bridge-free wave-soldered 0.5-mm-pitch 100-pin quad flat package (QFP) obtained with the Sn-0.7Cu-600 ppm Ni alloy.

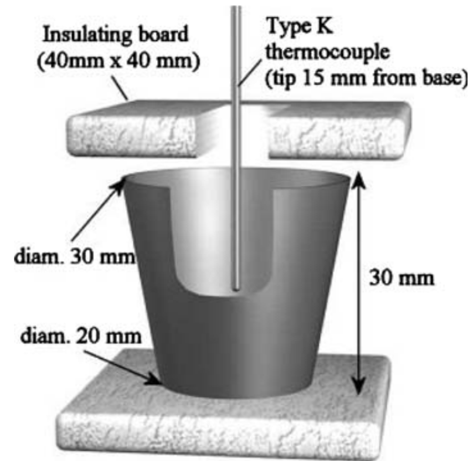

Fig. 2. A schematic (cut away and exploded for clarity) of the experimental set-up for thermal analysis. Two samples were taken simultaneously, one with and one without the thermocouple.

solderability of Sn-0.7Cu-xNi using microstructural analysis and fluidity length measurements.

EXPERIMENTAL PROCEDURE

Eleven Sn-0.7Cu-xNi alloys with nickel contents in the range of 0–1,000 ppm were studied. The alloys were prepared by mixing ingots of Sn-0.7Cu and Sn-0.7Cu-1,000 ppm Ni in clay-graphite crucibles and heating in an electric resistance furnace to a temperature of 350°C. The mean chemical compositions of the alloys were then confirmed by X-ray fluorescence (XRF) analysis; the measured compositions are given in Table I.

For microstructural observations, samples were collected from the melt in boron-nitride-coated stainless-steel cups, with dimensions given in Fig. 2. Two samples were taken simultaneously, placed on an insulating board, and then covered by another insulating board as depicted in Fig. 3. A thermocouple was placed in one sample to monitor the cooling curve as both samples cooled in air. For all alloys, the cooling rate in the liquid just prior to nucleation of the first solid was about –0.5°C/s. The samples without thermocouples were used for microstructural analysis. They were sectioned with a band saw, mounted in epoxy resin and then ground using SiC papers (180 and 220 grit) and diamond suspensions (9, 6, and 3 μm). The final polishing step was performed in a mixture of 96% OPS (0.05 μm colloidal silica), 2% ammonium hydroxide, and 2% hydrogen peroxide (30%) to slightly etch the Sn and improve the contrast for optical microscopy observations.

In order to analyze the composition of the intermetallics observed in metallographic sections, the Sn-0.7Cu-600 ppm Ni alloy was studied using several methods. A JEOL 6460LA scanning electron microscope was used for energy dispersive spectroscopy (EDS) measurements. Electron probe X-ray microanalysis (EPMA) was carried out in a JEOL JXA8200 microprobe. Finally, a method for elemental mapping using synchrotron X-ray fluorescence (μ-XRF) was used. The method has been developed at the synchrotron radiation light source

Table I. Compositions of the Alloys Studied in this Work Measured by XRF Analysis. Compositions are in wt.%.

Sample	Sn	Cu	Ni	Ag	Pb	Sb	Zn	Al	Fe
0 ppm Ni	Bal.	0.68	0.002	<0.005	0.04	<0.005	<0.005	<0.005	0.004
100 ppm Ni	Bal.	0.67	0.009	<0.005	0.03	0.006	<0.005	<0.005	0.004
250 ppm Ni	Bal.	0.67	0.025	<0.005	0.03	0.006	<0.005	<0.005	0.004
300 ppm Ni	Bal.	0.68	0.030	<0.005	0.03	0.01	<0.005	<0.005	0.009
350 ppm Ni	Bal.	0.67	0.034	<0.005	0.03	0.006	<0.005	<0.005	0.003
400 ppm Ni	Bal.	0.67	0.038	<0.005	0.03	0.006	<0.005	<0.005	0.003
500 ppm Ni	Bal.	0.67	0.047	<0.005	0.03	0.006	<0.005	<0.005	0.003
600 ppm Ni	Bal.	0.67	0.058	<0.005	0.02	0.007	<0.005	<0.005	0.005
700 ppm Ni	Bal.	0.67	0.064	<0.005	0.02	0.006	<0.005	<0.005	0.004
800 ppm Ni	Bal.	0.67	0.074	<0.005	0.02	0.006	<0.005	<0.005	0.003
1,000 ppm Ni	Bal.	0.67	0.092	<0.005	0.02	0.006	<0.005	<0.005	0.003

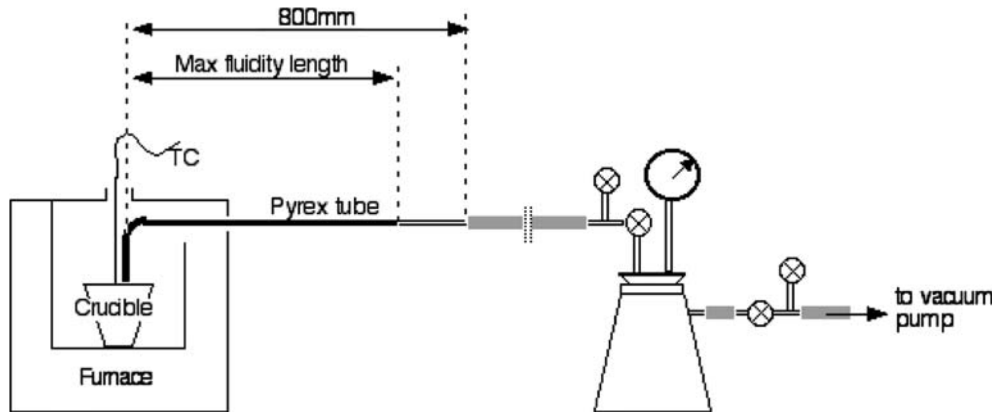

Fig. 3. Schematic illustration of the test apparatus for measurement of the fluidity length.

SPring-8, Japan.[15] The spatial resolution is sub-100 nm order, which is comparable to current FE-SEM/EDX resolution. The μ-XRF experiment was performed at undulator beamline 47XU at SPring-8, Japan. The detailed experimental procedure is described elsewhere.[15] The Ni Kα (7.471 keV) and Cu Kβ (8.904 keV) peaks were only present in the XRF spectrum from the Sn-0.7Cu-0.06Ni alloy and not in the reference Sn sample, and were therefore used for the elemental analysis.

Fluidity length measurements were carried out by the vacuum fluidity test method (Ragone method[14]), using the experimental arrangement shown in Fig. 3. 1,510 g of alloy was melted in a boron-nitride-coated clay-graphite crucible and held at the desired test temperature of 300.5°C (±0.4°C) in an electrical resistance furnace for at least 40 min to thermally equilibrate the system. A pressure difference of 50 kPa (±2 kPa) was applied to draw the molten metal into a Pyrex glass tube protruding horizontally out of the furnace. Because of heat loss along the glass tube, the molten metal loses its superheat and starts to solidify at some distance along the tube. Flow continues during solidification until the developing microstructure arrests flow.[13] Once solidification is complete, the length of the metal in the tube is measured; the maximum fluidity length is defined in Fig. 3. The experiment was repeated six times for each alloy composition.

RESULTS AND DISCUSSION

Microstructural Observations

Optical micrographs of the Sn-0.7Cu-xNi alloys from the experiments in Fig. 3 are shown in Fig. 4 a–h. The binary Sn-0.7Cu alloy is hypoeutectic, containing primary β-Sn dendrites separated by a eutectic microstructure consisting of β-Sn and Cu_6Sn_5 (Fig. 4a). In this binary alloy, the intermetallic phase appears as short laths. Nickel additions in the range 200–1,000 ppm caused significant changes in the microstructure (Fig. 4c–h). At an addition level of 200 ppm Ni, two types of microstructure were observed: some regions contained a microstructure with primary β-Sn dendrites (Fig. 4 b), similar to that in the Ni-free alloy, whereas other regions contained a more uniform eutectic microstructure (Fig. 4c). With increasing Ni additions (Fig. 4a-h), the volume fraction of β-Sn dendrites decreases and the intermetallic phase becomes coarser than the Cu_6Sn_5 in the binary alloy of Fig. 4a. All alloys also contained eutectic regions which appeared similar to those in the binary Sn-0.7Cu alloy.

The Ni-containing alloys additionally contained a microstructural feature which we term “coral zones” in this work (Fig. 5). Coral zones contain significantly smaller intermetallics than the lath-shaped intermetallics in Fig. 4a–h, as shown in the SEM images in Fig. 6a and b. The coral zones also usually display a complex internal structure with a cellular appearance.

To assess the change in coral zones with Ni content, a simple method was developed: Two samples of each alloy composition, representing a total surface area of 1,500 mm^2, were examined under an optical microscope. All coral zones present in the cross-sections were identified and the surface area of each coral zone was measured as indicated in Fig. 7. The results are shown in Table II and Fig. 8. The number of corals seems to increase with Ni content, and the area fraction appears to be highest for 300–600 ppm Ni alloys. We have observed similar features in a Sn-0.9Cu alloy, therefore suggesting that corals are related to early eutectic growth. The origin of corals is not understood at this stage, but it could be speculated that they form as a result of rapid eutectic growth occurring during the condition of relatively large undercooling during recalescence. Understanding the origin of corals could shed further light on the solidification mechanisms and phase relations in this alloy system.

The Sn-Cu_6Sn_5 binary eutectic composition is reported to be Sn-0.9wt.%Cu in the Thermocalc® solder database.[16] Assuming this eutectic composition and a partition coefficient of k = 0.066, the

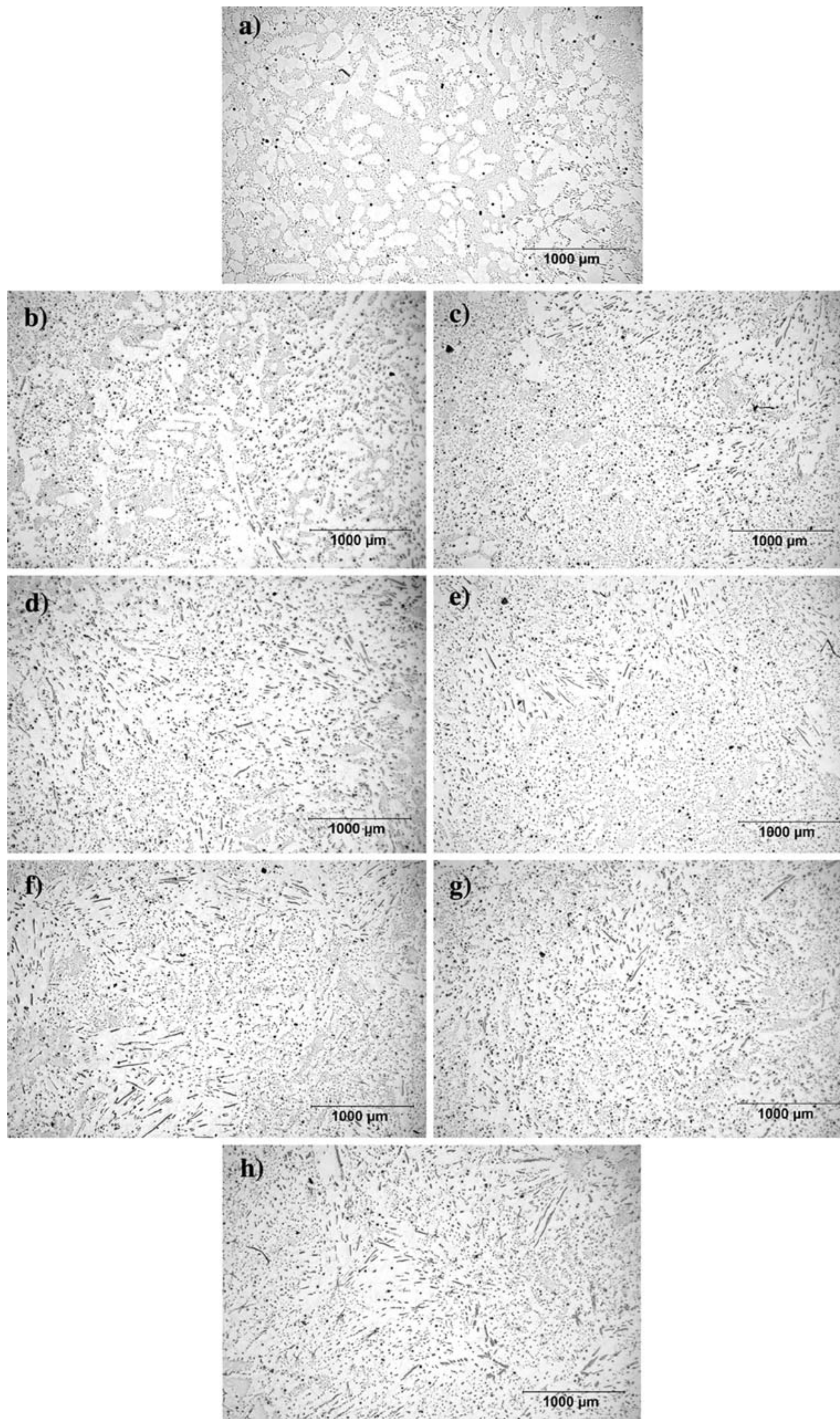

Fig. 4. Micrographs of Sn-0.7wt.%Cu with different Ni contents: (a) 0 ppm Ni, (b) 200 ppm Ni (region showing a microstructure with primary dendrites), (c) 200 ppm Ni (region with a more-uniform eutectic structure), (d) 300 ppm Ni, (e) 400 ppm Ni, (f) 500 ppm Ni, (g) 600 ppm Ni, and (h) 800 ppm Ni.

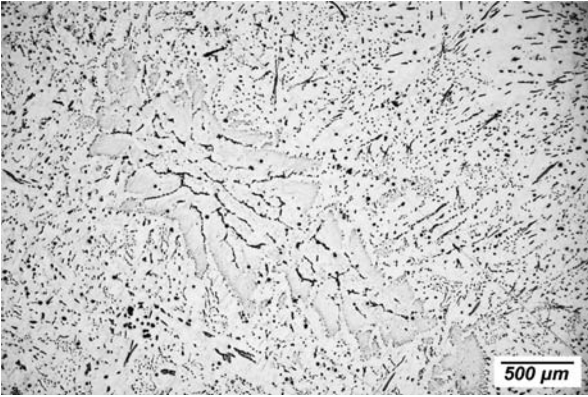

Fig. 5. Microstructural feature termed a "coral zone" (comprised of very fine intermetallics and with a cellular internal morphology) in a Sn-0.7Cu-0.05Ni sample.

volume fraction of primary β-Sn in Sn-0.7Cu is predicted to be 20% by the Scheil-Gulliver model. The hypoeutectic microstructure in the binary Sn-0.7Cu alloy in Fig. 4a is similar to this predicted primary phase fraction. At present, the Sn-rich end of the Sn-Cu-Ni ternary phase diagram is not well established,[17] although the salient features of the different suggested liquidus projections can be used to understand the microstructures in Fig. 4c–h. The ternary liquidus projection of Snugovsky et al.[18] suggests that Ni additions in the range 0–1,000 ppm Ni are significant compared to the phase diagram. Furthermore, their projection suggests that Ni additions to Sn-0.7Cu move the ternary composition towards a monovariant valley, consistent with the decreasing volume fraction of primary β-Sn with increasing Ni content in Fig. 4c–h. However, further studies are required to confirm the phase equilibria in Sn-rich Sn-Cu-Ni alloys because Lin et al.[19] propose a liquidus projection containing different phases to Snugovsky et al.[18] and the two sets of researchers also propose different types of invariant reactions.

The ternary liquidus projections of Snugovsky et al.[18] and Lin et al.[19] suggest that Ni additions to Sn-0.7Cu move the composition in the direction of a monovariant valley or an invariant point, both of which would involve the formation of an additional intermetallic phase. Based on this, the compositions of intermetallics with different morphologies were examined to study whether coarse, fine, and coral-zone intermetallics have different compositions.

EDS and EPMA point analysis sometimes detected Ni within the intermetallic phase(s), and detected no nickel in the β-Sn phase. However, neither method was able to discern any significant differences in composition between the fine, coarse, or coral-zone intermetallics due to significant scatter in the results. The main problem is the fineness of some intermetallics, particularly in the coral zones, with the volume of the electron beam detecting some Sn from the surrounding matrix. It is therefore not possible to comment on the reaction sequences predicted by the liquidus projections of Refs. 18 and 19 at this stage.

Typical EDS elemental mapping analysis are shown in Figs. 9 and 10, where it can be observed that Ni was detected in the intermetallics of Fig. 9 but not in that of Fig. 10. To determine whether the

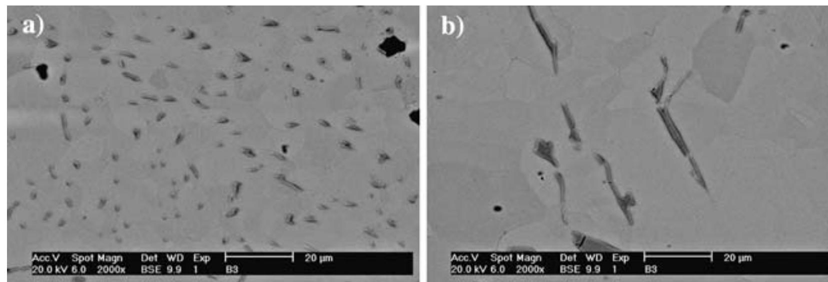

Fig. 6. High-magnification SEM images of Sn-0.7Cu-0.06Ni showing: (a) the intermetallics within the coral zone and (b) the typical, much larger, intermetallics with lath-shaped morphology outside of the coral zones.

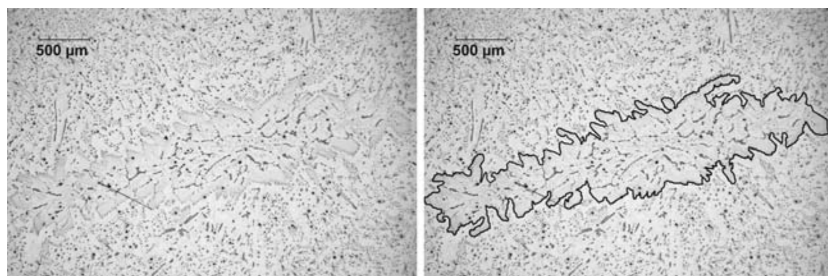

Fig. 7. Measurement of the coral zone surface area.

Table II. Number of Corals and their Total Surface Area Fraction for Different Sn-0.07wt.%Cu-*x*Ni Alloys Measured Across an Area of 1500 mm^2.

Ni Content (ppm)	# of Corals	Corals Total Surface (mm^2)	Surface Fraction (%)
0	0	0.00	0.00
200	14	16.07	1.07
300	26	55.23	3.68
400	30	52.71	3.51
500	71	66.07	4.40
600	44	58.94	3.93
800	38	39.49	2.63

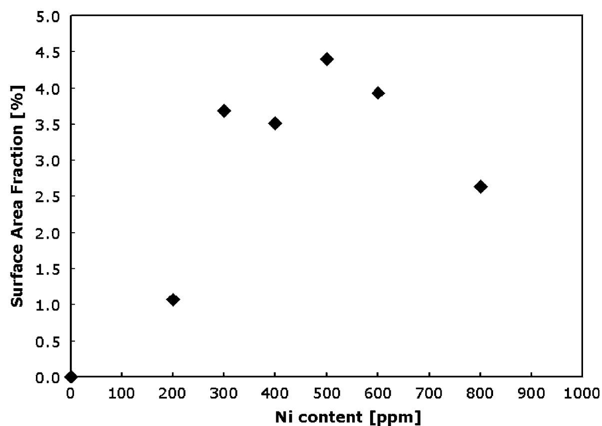

Fig. 8. Coral zone area fraction as a function of Ni content in Sn-0.7 Cu-*x*Ni.

intermetallic in Fig. 10 is nickel free, or whether the measurement was a result of inaccuracies in and detection limits of the EDS elemental mapping analysis, a higher-precision elemental mapping analysis was obtained using synchrotron radiation. Figure 11 shows synchrotron μ-XRF results from the same intermetallic as that in Fig. 10. It is readily apparent that μ-XRF was able to detect Ni in this intermetallic while EDS did not. Furthermore, the μ-XRF result demonstrates that nickel is present throughout the intermetallic phase. This result shows that care must be exercised when collecting and interpreting elemental analysis of intermetallics in these alloys.

Maximum Fluidity Length

Figure 12 shows the fluidity results for the different Sn-0.7Cu-*x*Ni alloys. The maximum fluidity length of Sn-0.7Cu-*x*Ni alloys is sensitive to small Ni additions. The fluidity length is lowest in the Ni-free alloy and varies only slightly with increasing Ni content until a threshold of 300–400 ppm Ni, after which the fluidity length increases markedly. The peak in fluidity length occurs in the region 500–600 ppm Ni. Further Ni additions lead to a gradual decrease in the fluidity. For the maximum nickel concentration studied (1,000 ppm Ni), the fluidity length is similar to Sn-0.7Cu-*x*Ni containing less than 350 ppm Ni.

It is well established in the literature that maximum fluidity length is a strong function of alloy composition, and that eutectic compositions have a longer fluidity length than off-eutectic alloys in most alloy systems.[13,14,20] The improved fluidity at

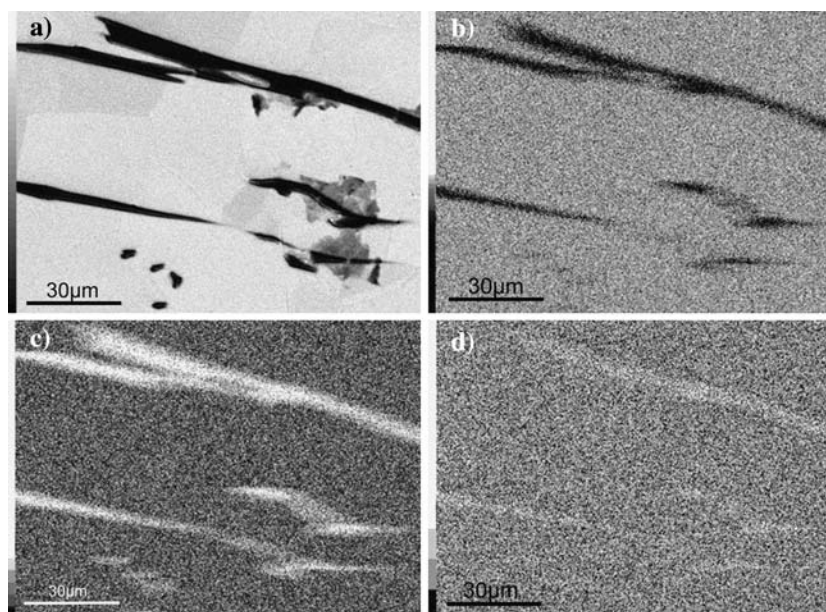

Fig. 9. Sn-0.7Cu-0.06Ni: (a) secondary-electron SEM image; elemental mapping results by EDS for: (b) Sn, (c) Cu and (d) Ni. Only a small amount of Ni was detected in the intermetallics.

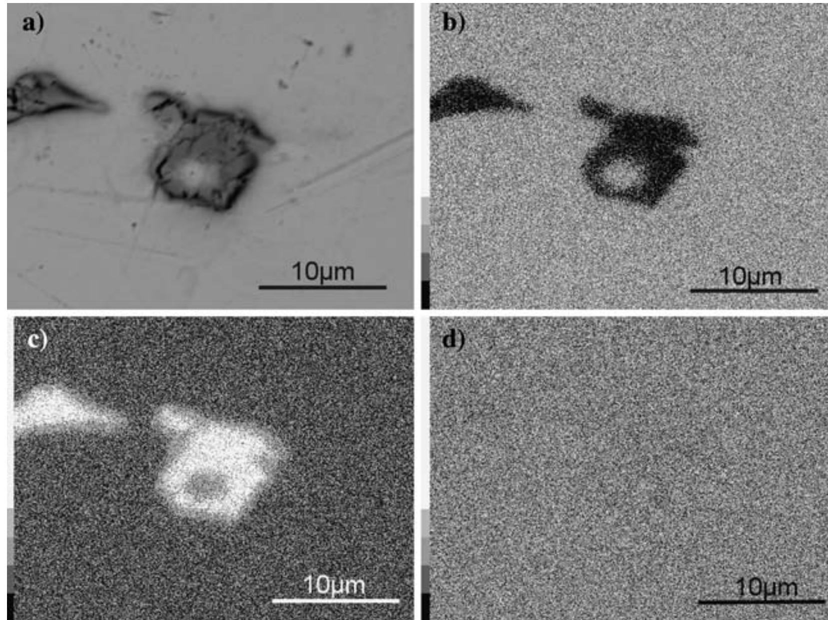

Fig. 10. Sn-0.7Cu-0.06Ni: (a) secondary electron SEM image; elemental mapping results by EDS for (b) Sn, (c) Cu and (d) Ni. No Ni was detected.

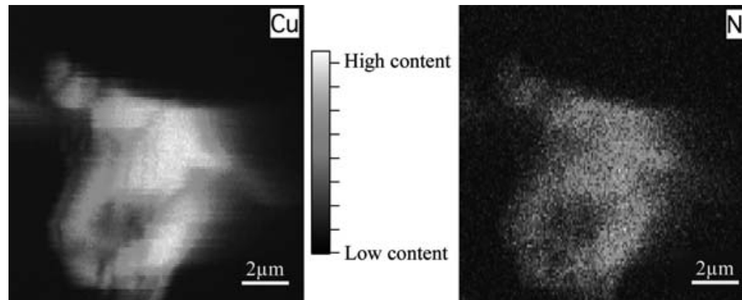

Fig. 11. Elemental mapping results for Cu and Ni in the Sn-0.7Cu-0.06Ni alloy, obtained by μ-XRF in synchrotron with 100 nm scan pitch and 0.3 s integration time.

eutectic compositions is usually explained by a smoother and more-planar solidification front, as opposed to the mushy columnar or equiaxed solidification modes for other alloy compositions. It is therefore probable that the peak in fluidity observed for 500–600 ppm Ni in Sn-0.7Cu alloy is caused by the suppression of β-Sn dendrites and the stabilization of a eutectic microstructure. A more-detailed study and description about fluidity of Sn-base solders is presented by Gourlay et al.[20]

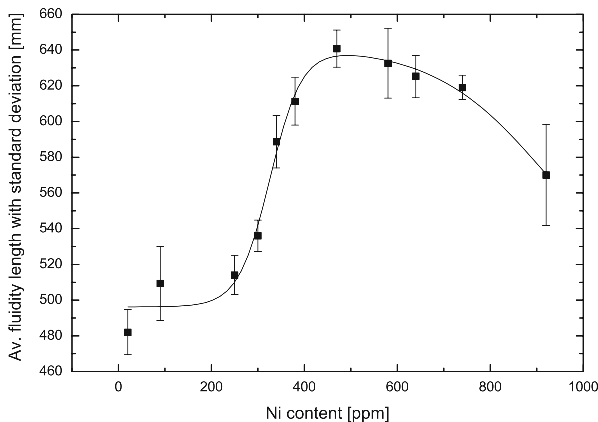

Fig. 12. Average fluidity length versus Ni content for Sn-0.7Cu-*x*Ni.

CONCLUSIONS

The addition of 0–1,000 ppm Ni to Sn-0.7Cu has been shown to significantly alter the microstructure of Sn-0.7Cu-xNi alloys. Ni additions were found to decrease the volume fraction of primary β-Sn dendrites, and to alter the appearance of intermetallics. In Ni-free alloys, the intermetallics are Cu_6Sn_5 laths. In Ni-containing alloys, intermetallic laths were coarser and the microstructures additionally contained much finer intermetallics incorporated into coral zones. EDS and EPMA analysis in an

SEM revealed that the Ni is present in some intermetallics, but not in the β-Sn phase. A synchrotron μ-XRF study of an intermetallic, which EDS measured to be Ni-free, revealed that Ni is concentrated throughout the same intermetallic, highlighting inaccuracies in determining the Ni distribution in these alloys by EDS measurements. An investigation into composition differences between the different intermetallic morphologies proved inconclusive.

Maximum fluidity length measurements showed that the flow behavior of solidifying Sn-0.7Cu-xNi alloys is sensitive to small nickel additions. A peak in maximum fluidity length was measured at 500 ppm Ni. The fluidity length measurements correlated well with the microstructural observations, similar to past studies on fluidity in solidifying alloys: alloys containing a significant fraction of primary dendrites exhibited the lowest fluidity length and the more fully eutectic microstructures exhibited the longest fluidity lengths.

ACKNOWLEDGEMENTS

The authors would like to thank Nihon Superior Co. Ltd., Japan, for providing the alloys. Fluidity experiments were supported by Mr. Bastian Meylan, The University of Queensland. Synchrotron experiments were performed at SPring-8 supported by the Ministry of Education, Culture, Sports, Science and Technology, Japan (Proposal No. 2006A1645/BL No. 47XU). The authors acknowledge the experimental support with the synchrotron study from Prof. H. Yasuda and Mr K. Yoshida, Osaka University, and Drs. K. Uesugi, A. Takeuchi, and Y. Suzuki, Japan Synchrotron Radiation Research Institute.

REFERENCES

1. Y. Li, K.-S. Moon, and C.P. Wong, *Science* 308, 1419 (2005).
2. C.M.L. Wu, D.Q. Yu, C.M.T. Law, and L. Wang, *Mat. Sci. Eng. R* 44, 1 (2004).
3. K. Suganuma, *Curr. Opin. Solid State Mater.* 5, 55 (2001).
4. I.E. Anderson, J.C. Foley, B.A. Cook, J. Harringa, R.L. Terpstra, and O. Unal, *J. Electron. Mater.* 30, 1050 (2001).
5. D.R. Frear, J.W. Jang, J.K. Lin, and C. Zhang, *JOM* 53(6), 28 (2001).
6. K. Suganuma, MRS BULL (Nov 2001).
7. M. Abtew and G. Selvaduray, *Mat. Sci. Eng. R* 27(5–6), 95 (2000).
8. C.M.L. Wu, D.Q. Yu, C.M.T. Law, and L. Wang, *J. Electron. Mater.* 31, 928 (2002).
9. S.H. Huh, K.S. Kim, and K. Suganuma, *Mater. Trans.* 42, 739 (2001).
10. T. Nishimura, in International patent EP1043112 (1999).
11. T. Nishimura, in US patent US6180055 (1999).
12. T. Nishimura, *Mater. J.* 43, 651 (2004).
13. M.C. Flemings, *Solidification Processing* (New York: McGraw-Hill, 1974).
14. D.V. Ragone, C.M Adams, and H.F. Taylor, *Trans. AFS* 64, 640 (1956).
15. K. Nogita, H. Yasuda, K. Yoshida, K. Uesugi, A. Takeuchi, Y. Suzuki, and A.K. Dahle, *Scripta Mater.* 55, 787 (2006).
16. K.-W. Moon and W.J. Boettinger, *JOM* 56(4), 22 (2004).
17. S.-W. Chen, C.-H. Wang, S.-K. Lin, and C.-N. Chiu, *J. Mater. Sci. Mater. E* 18, 19 (2007).
18. L. Snugovsky, P. Snugovsky, D.D. Perovic, and J.W. Rutter, *Mater. Sci. Technol.* 22(8), 899 (2006).
19. C.H. Lin, S.W. Chen, and C.H. Wang, *J. Electron. Mater.* 31, 907 (2002).
20. C.M. Gourlay, J. Read, K. Nogita, and A.K. Dahle, *J. Electron. Mater.* doi:10.1007/s11664-007-0248-8.